CrystEngComm

Accepted Manuscript

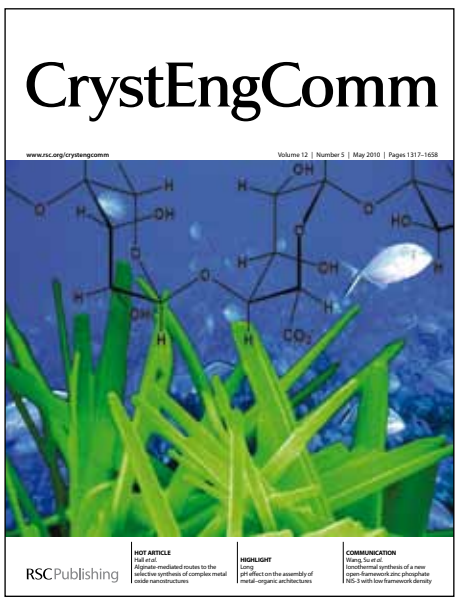

Experimental and theoretical analysis of *lp*…π intermolecular interactions in derivatives of 1,2,4-triazoles

Rahul Shukla[a], T. P. Mohan[b], B. Vishalakshi,[c] Deepak Chopra*[a],

[a]Department of Chemistry, Indian Institute of Science Education and Research Bhopal, Bhopal 462023, Madhya Pradesh, India.

[b]Rallis India Ltd, Bangalore 560091, Karnataka, India.

[c]Department of Chemistry, Mangalore University, Bangalore 574199, Karnataka, India.

Email: *dchopra@iiserb.ac.in*. Fax: 91-755-6692392.

Abstract

In the present study, we have synthesized and characterized two derivatives of biologically active 1, 2, 4-triazoles derivatives, a fluoro derivative, namely (*E*)-3-(4-fluoro-3-phenoxyphenyl)-4-((4-fluorobenzylidene)amino)-1-(morpholinomethyl)-1H-1,2,4-triazole-5(4H)-thione (**TRZ-1**) and a chloro derivative, namely (*E*)-4-((4-chlorobenzylidene)amino)-3-(4-fluoro-3-phenoxyphenyl)-1-(morpholinomethyl)-1H-1,2,4-triazole-5(4H)-thione (**TRZ-2**) *via* single crystal and powder X-ray diffraction. The chloro derivative crystallizes in the anhydrous (**TRZ-2A**) form and a solvated one (**TRZ-2B**) due to the presence of toluene molecule in the crystal. This solvatomorphic behavior has been studied in detail by different thermal techniques, namely DSC, TGA and combined with hot stage microscopy (HSM). All the three crystal structures show the presence of different intermolecular interactions of the type C-H…O, C-H…S=C, C-H…π, C-H…X (X= -F, -Cl) π…π and *lp*…π interactions. The fingerprints for all these interactions were evaluated using Hirshfeld surfaces. The nature and energetics associated with these interactions were characterized using PIXEL and supported by *ab initio* quantum mechanical calculations using TURBOMOLE. In addition, the calculations performed on the evaluation of the electrostatic potential render deeper insights into the nature of *lp*…π interactions.

Introduction

A detailed investigation of the nature of intermolecular interactions in crystals is an extremely important aspect of quantitative crystal engineering to facilitate the design of new materials with desirable properties [**1**]. The solid state architecture of molecules in crystalline solids, in the presence of strong donor and acceptors, is primarily controlled by the presence of various strong hydrogen bonds such as N-H…O/N, O-H…O/N respectively [**2**] and weak interactions such as C-H…O/N [**3**],

C-H…X (X= -F, -Cl, -Br, -I) [**4**], C-H…π [**5**] and π…π [**6**] interactions present in the crystal structures. In recent times, the anion/*lp*…π intermolecular interaction has became significantly important in supramolecular chemistry and biology [**7**]. The first report on this interaction was published by K. Hiraoka *et. al.* [**8(a)**] in which they discussed the interaction of different halogen anions with π system of hexafluorobenzene. Egli and Gessner were amongst the first who showed the importance of this interaction through their study on Z-DNA structure [**8(b)**]. Interestingly, *lp*…π interactions have also been observed in the study of RNA U-turns [**9**]. Recent experimental [**10**] and computational studies also reveal the importance of these interactions and their role in the stability of supramolecular and biomolecular entities [**11**]. A great deal of review work in this area also shows its importance [**12**].

Solvatomorphism, the counterpart of polymorphism, is a phenomenon in which a compound crystallizes with a variety of solvents [**13**]. Solvatomorphs are characterized by different molecular arrangements and exhibits a diverse array in molecular composition. Thermodynamic studies have shown that solvatomorphs can have different solubility and that can result in different chemical and biological activity of the compound, of importance in the pharmaceutical industry [**14**]. Although most of the organic compounds crystallize in the unsolvated form, because of entropic reason, the reason for their presence can be explained as the presence of a strong interaction between the solute and the solvent which makes the enthalpy consideration important resulting in the overall process being thermodynamically feasible [**15**]. It is often observed that the solvent fills the voids present in the crystal structure and may provide extra stability to the molecular assembly [**16**].

In the current study, two derivatives of 1, 2, 4-triazoles, namely (*E*)-3-(4-fluoro-3-phenoxyphenyl)-4-((4-fluorobenzylidene)amino)-1-(morpholinomethyl)-1H-1,2,4-triazole-5(4H)-thione (**TRZ-1**) and (*E*)-4-((4-chlorobenzylidene)amino)-3-(4-fluoro-3-phenoxyphenyl)-1-(morpholinomethyl)-1H-1,2,4-triazole-5(4H)-thione (**TRZ-2**) have been synthesized (**Scheme 1**) and characterized using ^{1}H-NMR, IR and PXRD respectively and these have been screened for the isolation of different forms. 1,2,4-triazoles and condensed triazole systems are reported to possess diverse types of biological activities such antifungal, antibacterial, antiparasitic, hypocholesteremic, hypotensive and anti-inflammatory properties [**17**]. Also, the derivatives containing the morpholine ring nucleus exhibit antimicrobial and antiurease activity [**18**]. The crystal structure analysis on these compounds has been performed. It is of interest to note that compound **TRZ-2** could be isolated as **TRZ-2A** and **TRZ-2B**, the latter containing toluene as a solvate. The crystal structures were found to be mainly stabilized by the presence of *lp*…π [O(*lp*)…π and S(*lp*)…π)] interactions in the absence of any strong hydrogen bonds and a quantitative assessment of the nature and energetics associated with these interactions is the

main focus of this article. These were evaluated via lattice energy calculations and an evaluation of the energetics associated with the different molecular pairs extracted from the crystal packing was made using PIXEL **[19]** and were also compared with the values obtained from *ab initio* calculations performed using TURBOMOLE **[20]**. The study is further supported by the analysis of Hirshfeld surfaces [**21(a)**] and the associated 2D fingerprint plots [**21(b)**] generated using CrystalExplorer 3.0 **[21(c)]**. The solvatomorphic behavior in **TRZ-2** was studied using DSC, TGA and HSM techniques.

Experimental Section:

Synthesis:

To a mixture of 4-substituted benzaldehyde (0.01 mol) and ethanol (15ml), an equimolar amount of 5-(4-fluoro-3-phenoxyphenyl)-4-amino-4H-1,2,4-triazole-3-thiol was added and then stirred and heated until a clear solution was obtained. In this clear solution, few drops of concentrated sulphuric acid were added and the resultant mixture was refluxed for 4 hours on a water bath and was left overnight at room temperature. The resultant precipitate was filtered and recrystallized from aqueous dimethylformamide to obtain 5-(4'-fluoro-3'-phenoxyphenyl)-4-(4"-substituted benzylideneamino)-4*H*-1,2,4-triazole-3-thiol **(A)**. The crystal structure of compound **(A)** has been determined by X-ray crystallography and it reveals that the compound exists in the thione form **[22]**. In the next step, (**A)** was added to a mixture of ethanol (15 ml), solution of formaldehyde (40%, 1.5 ml) and a secondary amine (morpholine) (0.01 mol) and the reaction was stirred and refluxed for thirty minutes and was left overnight at room temperature. The resultant precipitate was filtered and recrystallized from aqueous dimethylformamide to obtain the final product.

Scheme 1:

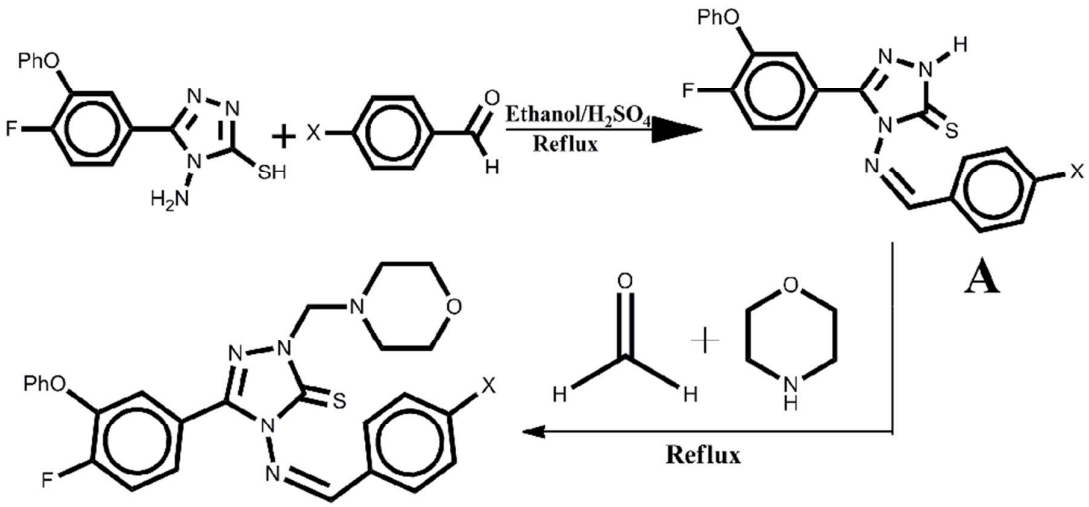

Crystal Growth

Suitable single crystals of **TRZ-1** and **TRZ-2** appropriate for X-ray diffraction measurements were obtained through solvent evaporation method. Crystals of **TRZ-1** and **TRZ-2** were obtained in toluene at room temperature. X-ray diffraction studies showed that the crystals of **TRZ-1** obtained from toluene were unsolvated while the crystal of **TRZ-2** in toluene contained the solvent molecule in its crystal structure. Subsequently, the unsolvated crystal of **TRZ-2** was obtained through solvent evaporation of the compound in 1:1 ratio of ethyl acetate: hexane at ~5°C.

Characterization

The yields of the final product, melting points of the compounds have been recorded and reported **(Table S2, ESI)**. All the synthesized compounds were characterized by FTIR **[Figure-S1 (a) –S1 (b), ESI]**, ^{1}H NMR **[Figure-S2 (a) – S2(b), ESI]**. The DSC traces for all the compounds (for determination of accurate melting points) were recorded on the powdered samples of all the synthesized compounds **[Figure-S3(a), ESI].**

In order to confirm the presence of a solvent molecule in **TRZ-2B**, DSC and TGA measurements was performed on both the solvated and anhydrous crystals of **TRZ-2B**. DSC analysis for a crystal of **TRZ-2A** shows an endothermic peak at 148.31˚C and for **TRZ-2B** shows an endothermic peak at 149.91˚ in the DSC plot **[Figure-S3(b), ESI]**. The similar value for these two peaks suggests that this corresponds to the melting point of the compound. In addition to this, **TRZ-2B** shows an additional peak at 95.46˚C, confirming the presence of the solvent molecule in the crystal structure of **TRZ-2B**. TG analysis performed on both **TRZ-2A** and **TRZ-2B** reveals difference in the weight loss till the melting point of ~150 ˚C is reached. **TRZ-2A** shows no weight loss up to the temperature of 150°C, indicating no decomposition of the sample, as compared to **TRZ-2B** which shows substantial weight loss before reaching the same temperature. It is of interest to note that after 150 ˚C, the nature of the TG curve is similar for both **TRZ-2A** and **TRZ-2B,** indicating decomposition of the sample. This proves that the initial weight loss in **TRZ-2B** (till the melting point) can be attributed to the loss of solvent molecule (**Figure-S4, ESI**).

In order to observe the physical changes during the process of heating, hot stage microscopy (HSM) experiments were performed on crystals of **TRZ-2B**. As evident from the optical images obtained from the experiment, the crystal shows a prominent change in physical appearance around 94.5˚C which corresponds to the loss of solvent and subsequently gets completely melted at 150˚C (no indication of decomposition), the onset of melting being 140 °C **(Figure-S5, ESI)**.

The products obtained was further characterized by experimental powder X-ray diffraction and compared with the simulated powder pattern generated from crystallographic coordinates **[Figure-S6(a)-6(b), ESI].** The phase purity of the product was established by refining the experimental profiles for the recorded powder diffraction pattern using the program JANA 2000 [**23**]. It is observed that the crystalline phase for **TRZ-1** and **TRZ-2A** are the same as the bulk phase **[Figure-S6(c)-6(d), ESI]**.

Data Collection, Structure Solution and Refinement:

Crystal data of **TRZ-1** was collected on Bruker D8 Venture four circle equipped with CMOS diffractometer using monochromatic Mo Kα (λ = 0.71073 Å) radiation at 100(2) K. The crystal data of **TRZ-2A** and **TRZ-2B** were collected on Bruker AXS SMART APEX CCD diffractometer using monochromatic Mo Kα (λ = 0.71073 Å) radiation at 100(2) K. Cell refinement and data reduction were performed using the program SAINT V7.685A12 (Bruker AXS,2009). The data were scaled and absorption correction was performed using SADABS V2008/112 (Bruker AXS). The crystal structures were solved with SIR 92 [**24**] and refined by least-squares methods on the basis of all observed reflections using SHELXL-97 [**25**] present in WinGx (version 1.80) [**26**]. All non-hydrogen atoms are refined with anisotropic displacement parameters. All the hydrogen atoms were then positioned geometrically and refined using a riding model with $U_{iso}(H) = 1.2U_{eq}[C(sp^2)]$ and $U_{iso}(H) = 1.5U_{eq}C(sp^3)$. The molecular connectivity was drawn using ORTEP-32 [**27**] and the crystal packing diagrams were generated using Mercury 3.1.1 program [**28**]. Geometrical calculations were done using PARST [**29**] and PLATON [**30**]. **Table-S3, ESI** lists all the relevant crystallographic and refinement data. Intermolecular interactions along with their interaction energies are listed in **Table-1**. The toluene molecule in **TRZ-2B** was observed to be disordered at two orientations with equal occupancy related by inversion axis. This was refined using the PART command in SHELXL-97.

Theoretical Calculations

Molecular structures were optimized by performing DFT calculation at the B3LYP/6-311G** using TURBOMOLE. The crystallographic coordinates were used as the starting geometry for the calculation. The experimentally obtained torsion angles were then compared with those in the isolated molecule (**Table-S4, ESI**). The lattice energy of all the compounds was calculated by the Coulomb-London-Pauli (CLP) computer program package [**31**]. The total lattice energy is partitioned into their coulombic, polarization, dispersion and repulsion contributions (**Table-2**). In CLP, the coulombic terms are handled by Coulomb's law while the polarization terms are calculated in the linear dipole approximation, the incoming electric field acting on local polarizabilities and generating a dipole with

its associated dipole separation energy; dispersion terms are simulated in London's inverse sixth power approximation, involving ionization potentials and polarizabilities; repulsion is represented as a modulated function of wavefunction overlap. Selected molecular pairs, extracted from the crystal packing, were analyzed with their interactions energies. The total interaction energy was then compared with the interaction energies obtained from the theoretical DFT+Disp calculations with the functional B97-D using an augmented basis set cc-pVTZ in TURBOMOLE (**Table-1**). DFT+Disp/B97-D method has found its application in calculating the interaction energies of non covalent interactions; particularly where dispersion component has a significant contribution [**32**]. The positions of the hydrogen atoms were moved to neutron values (1.08 Å for C-H) before the calculation. The basis set superposition error (BSSE) for the interaction energies was corrected (**Section-7, ESI**) by using the counterpoise method [**33**]. Electrostatic potential was also mapped using TURBOMOLE software with DFT/B3-LYP method using 6-311G** basis function and gOpenMol **[34]** graphical interface was used for visualizing the electrostatic potential map. The electrostatic potential was mapped on an isosurface of 0.0005 a.u. with the electrostatic potential ranging from 0.02 a.u. to -0.02 a.u**.**. Electrostatic potential were also plotted on the Hirshfeld surface. The *ab initio* wavefunctions for such plots were obtained using Gaussian 03 **[35]** with 6-31G** basis set **(Figure-6).**

Table-1: List of intermolecular interaction energies (kcal/mol) present in the three crystal structures. Cg1: N2-N4-C7-N3-C6, Cg3: C9-C14, Cg4: C15-20, Cg5: C21-C26, Cg6: Disordered toluene molecule.

Molecular Pair	D-H…A	D…A (Å)	H…A (Å)	D-H…A (°)	Symmetry Code	Centroid distance (Å)	E_{coul} (kcal/mol)	E_{pol} (kcal/mol)	E_{disp} (kcal/mol)	E_{rep} (kcal/mol)	E_{tot} (kcal/mol)	DFT-Disp/B97-D aug-cc-pVTZ (kcal/mol)
TRZ-1												
I	C19-H19…O2	3.536(4)	2.65	139	-1+x,y,z	6.333	-5.35	-2.46	-20.91	12.28	-16.42	-18.21
	C5-H5B…S1	3.941(4)	2.88	165	-1+x,y,z							
	C22-H22…F1	3.325(4)	2.33	152	-1+x,y,z							
	C9…C20(π…π)	-	3.504(4)	-	-1+x,y,z							
II	O1(*lp*)…C7(Cg1)	-	3.004(4)	-	1-x,-y,1-z	10.179	-4.18	-1.98	-12.88	8.26	-10.77	-13.37
III	C4-H4B…N4	4.060(3)	3.03	158	-x,-y,1-z	12.725	-2.29	-0.81	-7.52	4.75	-5.87	-6.84
IV	C6-S1(*lp*)…Cg3	4.273(3)	3.600(4)	102	2-x,-y,-z	8.050	-0.88	-1.84	-9.70	6.76	-5.66	-7.59
V	C11-H11…S1	3.961(3)	2.94	157	3-x, -y, -z	11.456	-2.15	-1.45	-5.61	4.03	-5.16	-4.57
VI	C1-H1B…F1	3.578(4)	2.55	158	x,-1+y,z	13.431	-1.55	-0.69	-6.02	3.63	-4.63	-5.44
	C2-H2A…Cg5	3.871(3)	2.95	143	x,-1+y,z							
VII	C25-H25…F2	3.815(5)	2.84	138	2-x,-1-y,-z	12.817	-0.35	-0.33	-4.87	1.53	-4.03	-4.43

VIII	O2(*lp*)…C18(Cg4)	-	3.187(4)	-	1-x,-1-y,1-z	9.199	-0.45	-0.43	-5.30	2.22	-3.99	-2.89
IX	C19-H19…F1	3.274(3)	2.34	143	-x,-1-y,1-z	12.066	-2.19	-0.59	-2.79	2.63	-2.96	-2.41
X	C24-H24…F2	3.303(3)	2.51	129	3-x,-y-1,-z	15.102	-1.36	-0.33	-2.58	1.43	-2.86	-2.89
XI	C23-H23…N1	3.766(5)	2.85	142	-1+x,1+y,z	14.760	-0.62	-0.35	-3.08	1.43	-2.63	-3.17
TRZ-2A												
I	C19-H19…O2	3.463(2)	2.61	135	-1+x,y,z	6.203	-5.99	-2.86	-25.38	15.77	-18.47	-18.94
	C5-H5B…S1	3.876(2)	2.82	165	-1+x,y,z							
	C22-H22…F1	3.398(2)	2.37	159	-1+x,y,z							
	C9…C20(π…π)	-	3.534(2)	-	-1+x,y,z							
II	*lp*(O1)…C7(Cg1)	-	3.004(2)	-	2-x,-y,1-z	10.659	-4.13	-1.98	-13.02	8.26	-10.87	-13.01
III	C6-S1(*lp*)…Cg3	4.333(3)	3.578(4)	105	3-x,-y,-z	8.035	-1.62	-1.95	-11.20	7.88	-6.90	-7.72
IV	C4-H4B…N4	3.989(3)	2.94	162	-1+x,1+y,z	13.173	-2.89	-1.14	-8.60	6.45	-6.28	-7.27
V	C11-H11…S1	5.522(3)	3.08	152	4-x,-y,-z	11.328	-1.67	-1.29	-6.95	4.18	-5.71	-4.66
VI	C1-H1B…F1	3.729(2)	2.71	156	x,-1+y,z	13.834	-2.34	-1.09	-6.35	4.87	-4.92	-5.60
	C2-H2A…Cg5	3.789(3)	2.94	136	x,-1+y,z							
VII	C24-H24…Cl1	3.482(3)	2.80	121	4-x,-1-y,-z	15.095	-2.00	-0.97	-5.76	4.42	-4.30	-2.33
VIII	C25-H25…Cl1	3.880(3)	2.92	148	3-x,-1-y,-z	13.002	-1.14	-0.57	-4.97	2.46	-4.23	-3.75
IX	O2(*lp*)…C18(Cg4)	-	3.137(4)	-	2-x,-1-y,1-z	9.437	-0.64	-0.59	-5.97	3.22	-3.99	-5.29
X	C19-H19…F1	3.463(2)	2.61	135	1-x,-1-y,1-z	12.407	-2.36	-0.57	-2.67	2.41	-3.17	-2.48
XI	C23-H23…N1	3.750(2)	2.82	143	-1+x,1+y,z	14.996	-0.69	-0.33	-3.15	1.45	-2.72	-3.21
TRZ-2B												
I	C19-H19…O2	3.549(2)	2.55	154	-1+x,y,z	6.567	-5.52	-2.39	-21.58	12.85	-16.65	-17.26
	C22-H22…F1	3.624(3)	2.57	164	-1+x,y,z							
	C5-H5B…S1	4.123(2)	3.07	163	-1+x,y,z							
	C9…C20(π…π)	-	3.423(4)	-	-1+,y,z							
II	O1 (*lp*)…C7(Cg1)	-	2.924(2)	-	-x,-y,2-z	10.229	-5.52	-2.48	-14.41	10.42	-11.99	-14.60
III	Cg3-Cg3	-	3.789(4)	-	-1-x,1-y,1-z	10.436	-0.71	-0.74	-9.91	4.89	-6.47	-6.84
IV	C4-H4B…N4	3.841(3)	2.85	151	1-x,-y,2-z	13.079	-2.98	-1.12	-8.62	6.45	-6.21	-6.45
V	C27-H27…Cl1	3.890(3)	2.91	151	-1-x,2-y,1-z	8.639	-1.88	-1.05	-6.81	5.04	-4.70	-3.97
	C24-H24…C29(Cg6)	3.955(3)	2.91	162	x,y,z							
VI	O2 (*lp*)…C18(Cg4)	-	3.105(4)	-	-x,1-y,2-z	9.274	-0.88	-0.62	-6.52	3.39	-4.63	-5.94
VII	C1-H1B…F1	3.624(3)	2.57	164	x,-1+y,z	13.504	-1.24	-0.54	-5.52	3.15	-4.15	-5.11
	C2A-H2A…Cg5	3.930(3)	3.00	148	x,-1+y,z							
VIII	C28-H28…S1	4.005(7)	3.08	144	-x,1-y,1-z	8.025	-2.96	-1.50	-5.23	5.59	-4.13	-4.32
	C30-H30A…S1	3.796(7)	2.79	153	-x,1-y,1-z							
IX	C11-H11…Cl1	3.855(3)	2.83	158	-2-x,1-y,1-z	15.105	-1.72	-0.90	-3.89	2.86	-3.65	-2.01
X	C23-H23…N1	3.554(3)	2.51	162	-1+x,1+y,z	14.974	-1.64	-0.71	-3.91	3.25	-3.05	-3.61
XI	C30-H30B…S1	4.002(7)	3.12	139	-1-x,1-y,1-z	7.841	-1.69	-1.17	-4.99	5.13	-2.72	-2.68

XII	C19-H19…F1	3.360(2)	2.53	133	1-x,1-y,2-z	12.398	-1.33	-0.35	-2.39	1.38	-2.70	-2.59

Results and Discussion:

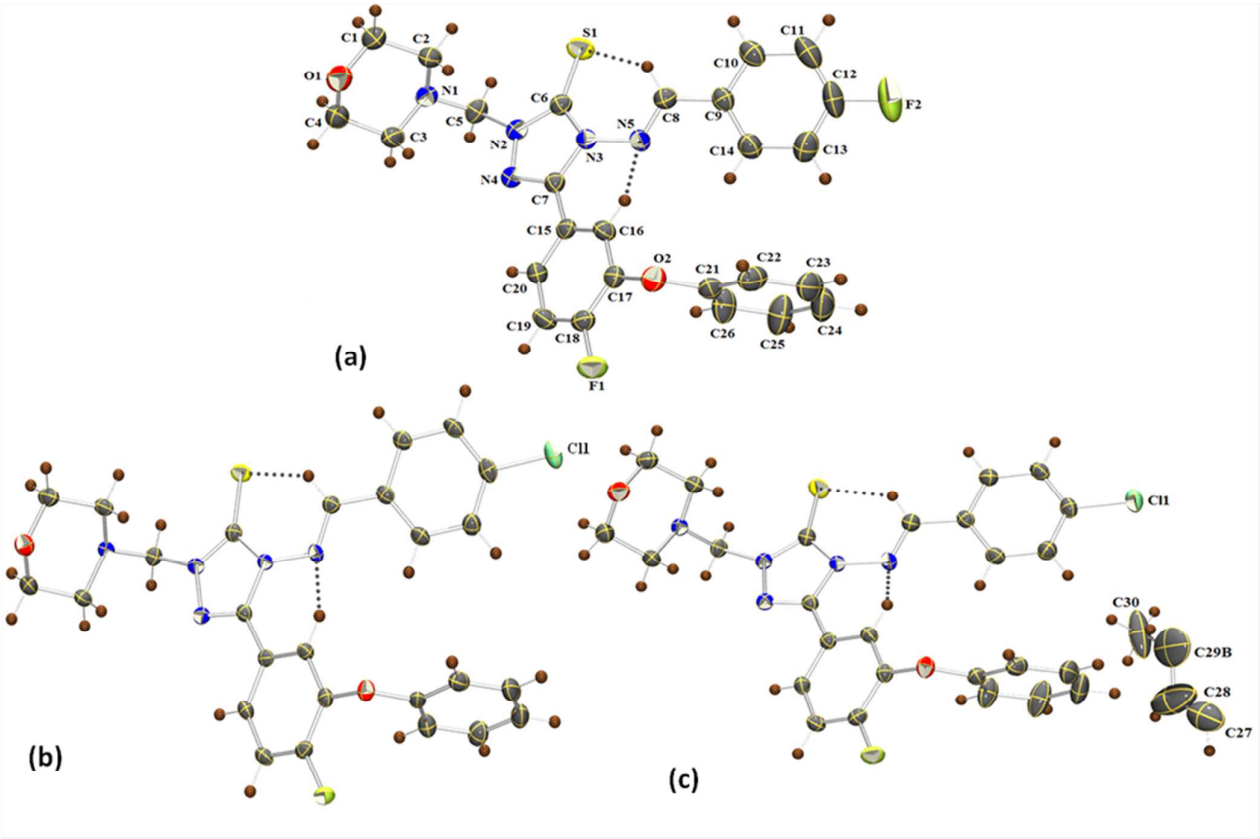

Figure-1: *ORTEP* diagrams drawn with 50% ellipsoidal probability of (a) **TRZ-1** with atom numbering scheme. The same scheme has been followed for all the structures. (b) **TRZ-2A** (c) **TRZ-2B** showing the half molecule of toluene in the asymmetric unit. Dotted lines depict C-H…S=C and C-H…N=C intramolecular interactions.

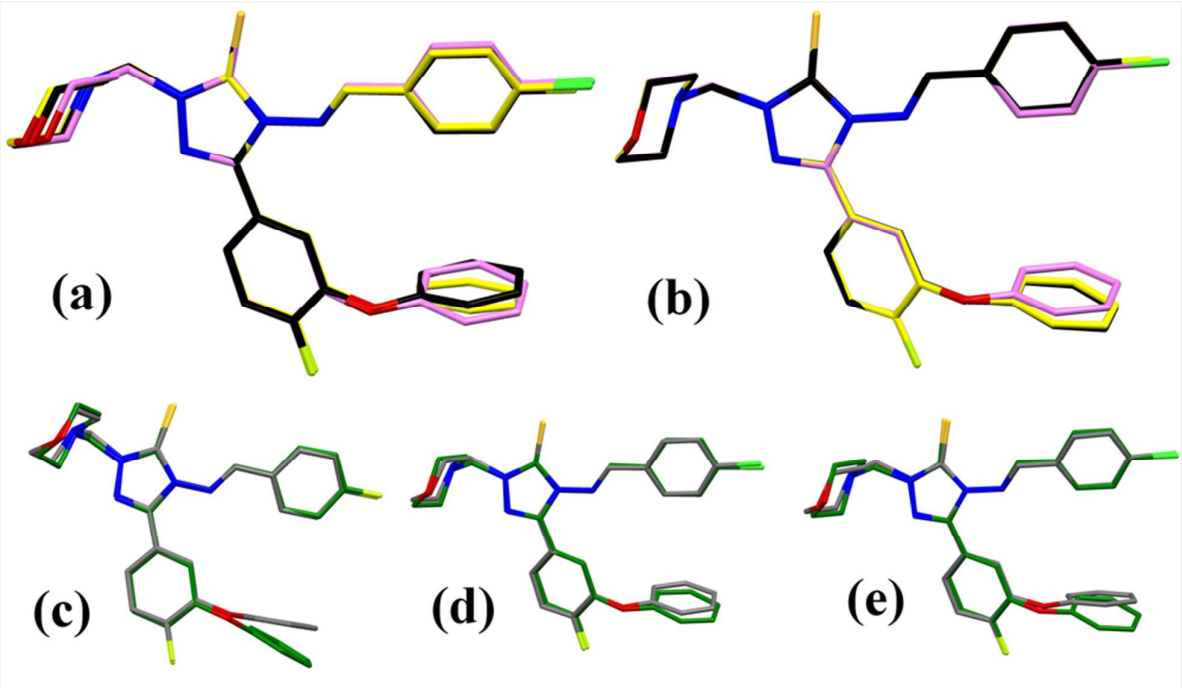

Figure-2: (a) Overlay diagram of **TRZ-1**(C-atoms are in black), (b) **TRZ-2A** (C-atoms in yellow), **TRZ-2B** (C-atoms in violet) at solid state geometry (b) for all the molecules at gas phase geometry. (c) the overlay diagram of the solid state geometry of **TRZ-1**, (in grey) respectively with their corresponding optimized geometry (in green). (d) the overlay diagrams of the solid state geometry of **TRZ-2A** (in grey) respectively with their corresponding optimized geometry (in green). (e) The overlay diagram of the solid state geometry of **TRZ-2**B (in grey) respectively with their corresponding optimized geometry (in green).

ORTEP diagrams for **TRZ-1**, **TRZ-2A** and **TRZ-2B** have been shown in **Figure-1**. All the compounds crystallized in *P*-1 symmetry with Z = 2. The asymmetric unit of **TRZ-2B** contains half molecule of toluene, the other half being related by an inversion center. The presence of a similarly disordered toluene molecule as a guest in clathrate behaviour is also reported in the literature **[36]**. The molecule can be divided into four different parts. The first part consists of the triazole ring, the second one consists of the flexible fluoro phenoxy group, the third part is the morpholine ring present and the last part consists of the halogen substituted phenylmethanimine. The molecular conformation in all three crystal structures is stabilized by the presence of an intramolecular C-H…S=C (involving H8 and S1) and C-H…N (involving H16 and N5) interaction in the solid state and this is also present in the isolated molecule **(Figure-2, Table-2)**. **Figure 2(c)-(e)** shows that the molecular geometry is nearly superimposable in the solid state and gas phase, the differences existing only in the phenoxy part of the molecule. The value for

the torsion angle suggests that except for torsion-3 (morpholine ring), 5, 6 (both correspond to the fluorophenoxy moiety), the remaining torsion angles were similar in the solid state **(Table-S4, ESI).**

Table-2: Intramolecular interactions present in the asymmetric unit. The value in italics are obtained from the optimized structures using DFT/6-311G** calculations.

C-H…A	**TRZ-1(Å)**	**TRZ-2A(Å)**	**TRZ-2B(Å)**
C8-H8…S1	2.46 *2.46*	2.51 *2.45*	2.44 *2.44*
C16-H16…N5	2.24 *2.44*	2.29 *2.45*	2.32 *2.45*

Both the molecules consist of similar type of hydrogen bond donor and acceptors atoms. Hydrogen atoms attached to sp^2 hybridized carbon atom and sp^3 hybridized carbon atom acts as weak hydrogen bond donor in both the molecules. **TRZ-2B** contains additional weak hydrogen bond donors because of the presence of the toluene molecule. In terms of acceptor atoms, **TRZ-1**, **TRZ-2A** and **TRZ-2B** contain three types of nitrogen atom. N1 is part of the morpholine ring, three nitrogens, namely N2, N3 and N4 are part of the triazole ring, N5 is connected to C8 *via* a double bond, having a localized lone pair. There are different oxygen atoms, namely O1, which is a part of the morpholine ring while O2 is connected to the aromatic ring forming the phenoxy part of the molecule. Both the oxygen lone-pairs are available for active participation. Apart from this, **TRZ-1** contains two fluorine atoms (F1 and F2) acting as a weak hydrogen bond acceptor. One fluorine atom (F2) present in **TRZ-1** is replaced by a chlorine atom as a possible hydrogen bond acceptor in **TRZ-2**. The molecules also contain aromatic π rings which can act as a weak hydrogen bond acceptor. Apart from these hydrogen bonds all the compounds also have the propensity of formation of other weak non covalent interactions such as π…π stacking, *lp*…*π* etc, hence leading to the greater competition amongst all the different kinds of intermolecular interactions (either strong or weak) in the formation of supramolecular assembly of the compounds.

The lattice energy calculations for all the three compounds are given in **Table-3**. Due to the presence of half toluene molecule in the asymmetric unit of **TRZ-2B** the lattice energy for **TRZ-2B** was calculated in accordance with the procedure reported in the literature [**37**]. The symmetry of the crystal structure was reduced to *P*1 symmetry and this leads to the presence of two molecules and a guest toluene molecule and hence a total three molecules in the asymmetric unit **[Figure-S7(a), ESI].** Since the module PIXEL is not able to perform the calculations in cases wherein more than two molecules

are present in the asymmetric unit and hence three different independent pairs were created. **Pair-1** consists of two host molecules present at different orientations **[(i) and (ii), Figure-S7, ESI]**. **Pair-2** consisted of one of the host molecule along with the solvent molecule **[(i) and (iii), Figure-S7, ESI]; Pair-3** consisted of the other host molecule with a solvent molecule **[(ii) and (iii), Figure-S7, ESI]**. The lattice energy calculations for all these pairs were performed separately and the values reported in **Table-3**.

Table-3: Lattice energy from CLP (in kcal/mol).

Comp. Code	E_{Coul}	E_{Pol}	E_{Disp}	E_{Rep}	E_{Tot}
TRZ-1	**-14.43**	**-6.33**	**-57.52**	**33.19**	**-45.12**
TRZ-2A	**-17.37**	**-7.74**	**-66.58**	**41.77**	**-49.90**
TRZ-2B	**-**	**-**	**-**	**-**	**-**
Pair-1	**-15.22**	**-6.21**	**-55.97**	**33.96**	**-43.45**
Pair-2	**-7.31**	**-3.34**	**-25.28**	**16.89**	**-19.04**
Pair-3	**-5.87**	**-2.65**	**-23.70**	**13.95**	**-18.28**

Quantitative Crystal Structure Analysis: Hirshfeld and XPAC study

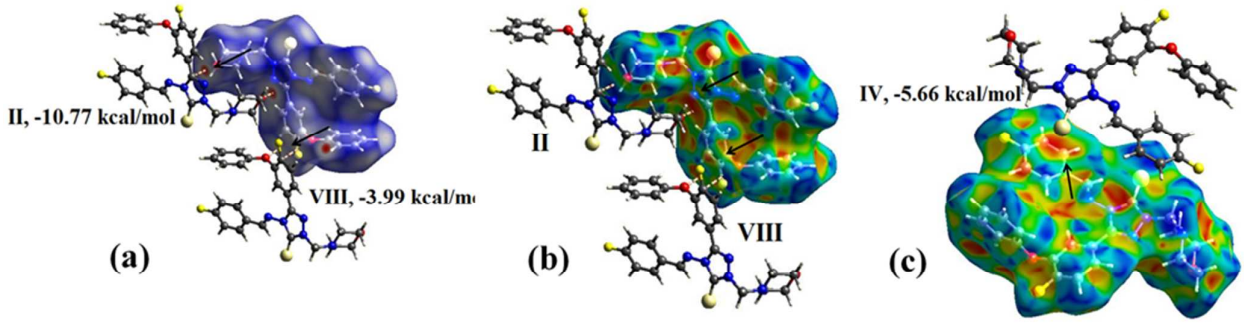

Figure-3: Hirshfeld surfaces mapped with d_{norm} and/or shape-index properties along with molecular pairs involving *lp*...π and their respective PIXEL interaction energies in **TRZ-1**.

The important packing motifs (molecular pairs) from the crystal structure have been extracted for a complete understanding of the nature of interactions with quantitative inputs from an evaluation of the interaction energy calculated from PIXEL and TURBOMOLE. Molecular pairs of **TRZ-1** with their corresponding interaction energies has been represented in **Figure-S9[(a)-(f), ESI]** along with their d_{norm} and surface-index properties. The most stabilized molecular pair in **TRZ-1 [**motif–**I]** consists of a short C-H…O interaction (involving H19 and O2), C-H…S=C interaction (involving H5B and S1), and a short C-H…F interaction (involving H22 and F1). It is well known that C-H…F intermolecular interactions contribute towards differences in polymorphism [**38**] and their presence is well recognised in molecular solids [**39**], including crystallization of liquids [**40**]. Along with these interactions, motif-

I also involves a stacking interaction (involving C9 of Cg3 ring and C20 of Cg4 ring) with C…C distance being 3.504(4) Å and hence resulting in total interaction energy of -16.42 kcal/mol. The combined nature of these interactions is mostly of a dispersive nature, the stabilization contribution being 75%. The presence of a red-blue triangle (marked with arrow) around the Cg4 region in the shape-index property **[Figure-S9(b), ESI]** confirms the presence of a stacking interaction. The second most stabilized molecular pair, motif-**II**, shows the presence of a *lp*...π interaction (involving C1-O1/C4-O1 and C7 atom of Cg1 ring), the interaction energy being -10.77 kcal/mol, the principal stabilization of around 75% corresponding to dispersion interactions. The presence of this interaction is confirmed by a large red spot in the property d_{norm} (marked with arrow in **Figure-3(a)**) and also by a corresponding red region in the shape-index property **[Figure-3(b)].** The **III** most stabilized interaction is a dimeric C-H…N interaction (involving H4B and more available lone pair of electrons on N4) with an interaction energy of -5.87 kcal/mol **[Figure-S9(a), ESI]**. The next most stabilized interacting motifs are **IV** and **V** involving the sulphur atom. **IV** corresponds to another *lp*…π interaction (involving C6-S1 and the Cg3 ring), and **V** corresponds to C-H…S interaction (involving H11 and S1) respectively**.** The interaction energy being -5.66 kcal/mol for **IV [Figure-3(a)]** and -5.16 kcal/mol **[Figure-S9(c), ESI]** for **V** respectively. The presence of a C=S…π interaction is confirmed by the presence of a red-blue triangle spot [marked with arrow in **Figure-3(c)**]. Motif-**VI** and **VII** both utilize weak C-H…F interactions in their molecular pairs. Apart from the presence of a short and directional C-H…F interaction (involving H1B and F1), **VI** also involves a C-H...π interaction (involving H2A and Cg5), the total interaction energy being -4.63 kcal/mol **[Figure-S9(a), ESI]**. **VII** is supported by the presence of a weak C-H…F interaction (involving H25 and F2), the interaction energy being -4.03 kcal/mol **[Figure-S9(e), ESI]**. Motif-**VIII** is stabilized by the presence of another *lp*…π interaction (involving C17-O2/C21-O2 and C18 atom of Cg4 ring) with a interaction energy of -3.99 kcal/mol [red spot in the shape-index property marked with arrow in **Figure-3(b)**]. **IX** involves the presence of a short and directional C-H…F interaction (involving H19 and F1) forming a dimer and having an interaction energy of -2.96 kcal/mol [the red spot in d_{norm} marked with arrow in **Figure-S9(a), ESI**]. **X** involves a single C-H…F interaction (involving H24 and F2) and has a stabilizing energy of -2.86 kcal/mol, being comparable to that of **IX [Figure-S9(c), ESI].** The least stabilized molecular pair i.e. **XI** involves a C-H…N interaction (involving H23 and available *lp* of electrons on N1) and having an interaction energy of -2.63 kcal/mol **[Figure-S9(e), ESI]**. The calculated energies obtained are comparable to those reported in the literature **[4, 41].** It is of interest to note that the strength of a given interaction depends on the nature of the interacting atoms which in turn is governed by the electron density distribution in the remaining molecule. It is noteworthy that weak interactions

may impart greater stabilization in the crystal environment, thereby delineating their contribution towards the crystal packing.

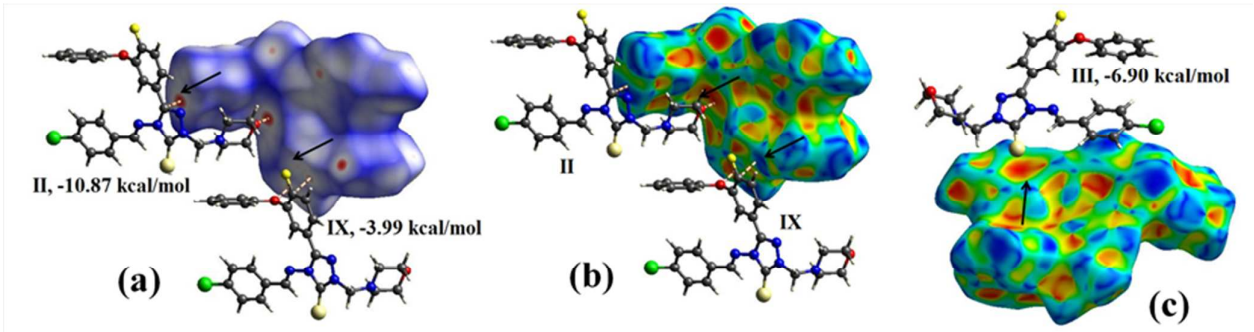

Figure-4: Hirshfeld surfaces mapped with d_{norm} and/or shape-index properties along with molecular pairs involving *lp*...π and their respective PIXEL interaction energies in **TRZ-2A**.

The molecular pairs extracted for **TRZ-2A** has been shown in **Fig-S10[(a)-(f), ESI]** with their respective interaction energies. The packing features of **TRZ-2A** were largely similar to those observed for **TRZ-1**. Furthermore, the energy of the three *lp*...π interactions of **TRZ-2A** was similar to those observed in **TRZ-1**[**Figure-4(a)-(c)** and **Table-1**]. The only difference between the two structures was the replacement of the fluorine atom F2 present in **TRZ-1** with a chlorine atom Cl1 in **TRZ-2**. Furthermore, it is observed that an interaction in which F2 was involved in **TRZ-1** was replaced by a similar interaction with Cl1 in **TRZ-2A** The molecular pairs in which the atom Cl1 is involved consists of motif-**VII,** a C-H…Cl interaction (involving H24 and Cl1) results in an energy stabilization of -4.30 kcal/mol **[Figure-S10(c), ESI].** The other molecular pair, motif-**VIII**, involving H25 and Cl1, with an interaction energy of -4.23 kcal/mol **[Figure-S10(e), ESI]** provides further stability. The nature of the C-H…Cl interactions is essentially of a dispersive nature, this contributing to 70% of the total stabilization. The presence of these two different C-H…Cl interaction is clearly evident from their corresponding shape –index property [**Figure-S10(d)** and **Figure-S10(f), ESI** respectively].

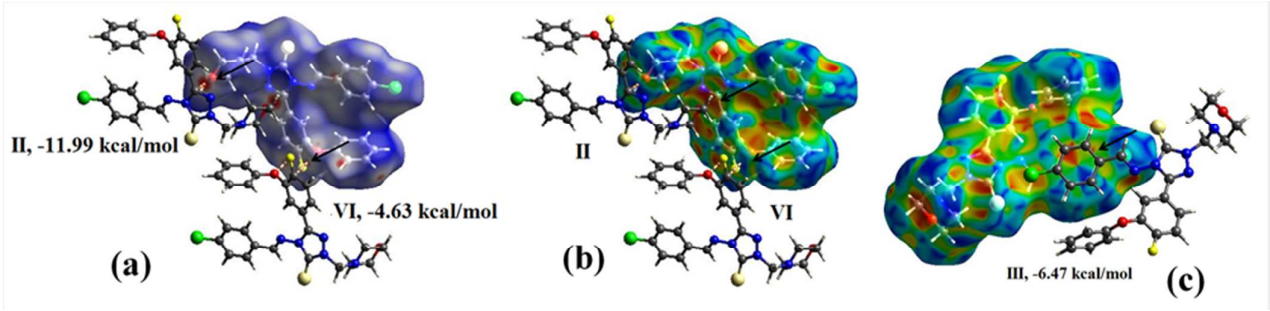

Figure-5: Hirshfeld surfaces mapped with d_{norm} and/or shape-index properties along with molecular pairs involving *lp*...π and their respective PIXEL interaction energies in **TRZ-2B**.

The extracted molecular pairs of **TRZ-2B** have been shown in **Fig-S11[(a)-(f), ESI]**. It is the solvated crystal of **TRZ-2** because of the presence of toluene as the solvent molecule. As evident from the packing diagram [**Figure-S13, ESI**] the solvent molecule is occupying the empty void space between the host molecules and connects two different layers of molecular assemblies. The solvent molecule is present in the close vicinity of the chlorine atom, Cl1 and sulphur atom, S1. In **TRZ-2B**, the interactions in which S1 and Cl1 are not involved are not altered by the presence of the solvent molecule and hence show similar interaction energies as those obtained for **TRZ-1** and **TRZ-2B (Table-1)**. In **TRZ-2B**, the Cg3 ring is involved in a π…π interaction (motif-**III**, interaction energy being -6.47 kcal/mol) as opposed to **TRZ-1** and **TRZ-2B** in which Cg3 ring was involved in C=S(*lp*)…π interaction. The corresponding shape-index plot for **III** (marked with arrow in **Figure-5(c)**) also confirms the presence of this stacking interaction. Furthermore, in **TRZ-2B**, molecular motif-**IX** was involved in a dimeric C-H…Cl interaction (involving H11 and Cl1) the energy stabilization being -3.65 kcal/mol. The presence of this interaction is evident from the corresponding d_{norm} property **[Figure-S11(c), ESI].** This interaction was not present in the **TRZ-2A**, as H11 was involved in an interaction with S1 atom. The presence of the solvent molecule eliminated the possibility of formation of related H…Cl and H…S interactions between the two host molecules. The stabilizing intermolecular interaction i.e. C24-H24…Cl1 that was observed in **TRZ-2A** were not evident in **TRZ-2B**. The disordered solvent molecule is actively involved in the formation of weak intermolecular interactions with the host molecule. The most stabilized host-guest interaction is represented by the molecular motif-**V**, which involves a C-H…Cl interaction (involving H27 and Cl1) and a C-H…π interaction (involving H23 and C29), the interaction energy being -4.70 kcal/mol. Presence of this interaction is confirmed by a red region around Cl1 atom in the corresponding shape-index property [**Figure-S11(e), ESI]**. The S1 atom is also participating with the guest solvent molecule giving rise to two different molecular pairs i.e. **VIII** and **XI**. Motif-**VIII** consists of two C-H…S interaction (involving H28, H30A with S1) having a stabilization energy of -4.13 kcal/mol **[Figure-S11(e), ESI].** Motif-**XI**, also consists of a single C-H…S interaction (involving H30B and S1) having a total stabilization energy of -2.72 kcal/mol **[Figure-S11(e), ESI].**

The presence of similar packing characteristics in **TRZ-1** and **TRZ-2** suggest the presence of isostructurality **[42]** in these molecules **[Section-6, ESI][43]**.It was observed from XPAC results that **TRZ-1/TRZ-2A** have a 3D structural similarity (isostructural) with a dissimilarity index **[44]** of 3.3. **TRZ-1/TRZ-2B** and **TRZ-2A/TRZ-2B** have a 2D structural similarity with a dissimilarity index of 5.7 and 7.5 respectively.

Quantitative Analysis of the Electrostatic Potentials (ESP) with relevance to *lp*…π interactions present in the crystal structures.

The 3D-ESP **[45(a)]** was mapped over the Hirshfeld Surface and the electron density isosurface in order to obtain quantitative insights into the nature of electron rich and electron deficient sites in the molecule. The ESP on the Hirshfeld surface [**45(b)**] was plotted in the range of 0.05 a.u.(blue) to -0.05 a.u.(red). Similarly the ESP plotted using gOpenMol was plotted on an isosurface of 0.0005 a.u. with potential ranging from 0.02 a.u.(blue) to -0.02 a.u.(red). The separation of electronegative and electropositive regions is well demonstrated in the ESP map. As expected in all the three molecules, the electronegative regions are spread around the oxygen, nitrogen and sulphur atom. The most significant difference between **TRZ-1** in comparison to **TRZ-2A** and **TRZ-2B** was the formation of the σ-hole around the chlorine atom in **TRZ-2A** and **TRZ-2B [**marked with arrow in **Figure-6(a)]**. The existence of a σ-hole is well-documented in the literature **[46]** and its existence suggests an anisotropic distribution of the electron density around the chlorine atom **[47]**. The shape and size of the electrostatic region around the Cl atom is different in **TRZ-2A** and **TRZ-2B [Figure-6(b)]**.

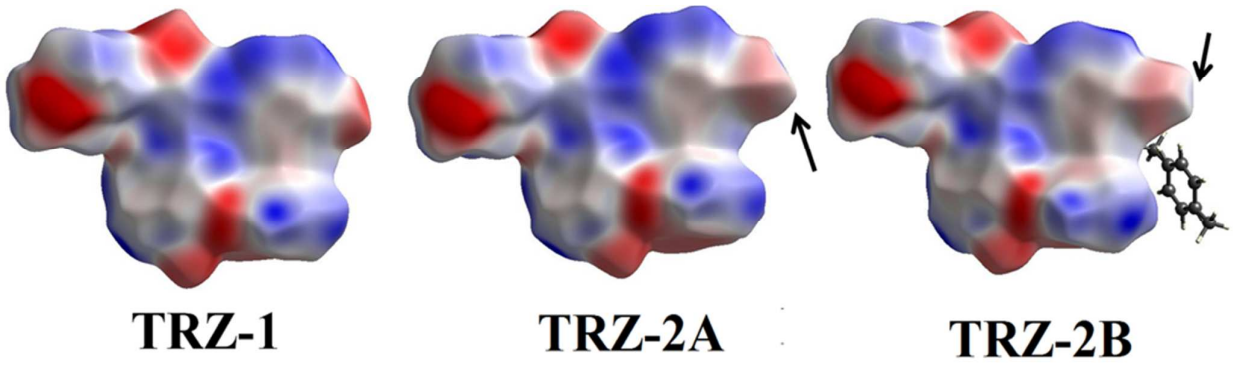

Figure-6(a): ESP plotted on the Hirshfeld Surface. All the ESPs were mapped on the molecular surface in the same orientation as those represented in the *ORTEP* diagram. The ranges of ESP are from 0.05 a.u.(blue) to -0.05(red).

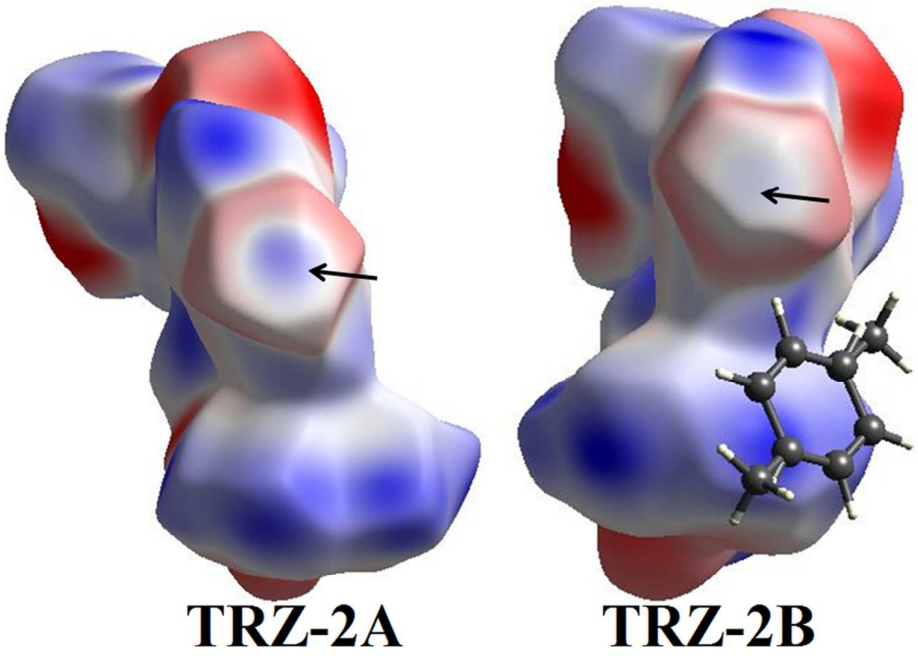

Figure-6(b): Image depicting the formation of σ-hole in **TRZ-2A and 2B** (marked with arrows). ESP mapped on the Hirshfeld isosurface ranging from blue (0.05 a.u.) to red (-0.05 a.u.).

The stability of the *lp*…π interactions was also analysed through decomposition of ESP mapped on the Hirshfeld surface. In **TRZ-1**, the O_{ethoxy} had an electronegative region with a potential value being -0.08 a.u., interacting with the electropositive region of Cg1 ring with potential value being +0.04 a.u giving rise to O1(*lp*)…C7(Cg1) interaction **[Figure-7]**. In case of O2(*lp*)…C18(Cg4) interaction in **TRZ-1**, the strength of the electronegative region (-0.04 a.u.) and the corresponding electropositive region (+0.01 a.u) was less pronounced as compared to O1(*lp*)…C7(Cg1) interaction, hence leading to a comparatively weaker interaction. This feature of the ESP is in full accord with the observed interaction energy (for **TRZ-1** the values being -10.77 and -3.99 kcal/mol) **(Table-1)**. Similar trends for both O(*lp*)…π interaction was observed in both the **TRZ-2A** and **TRZ-2B**.

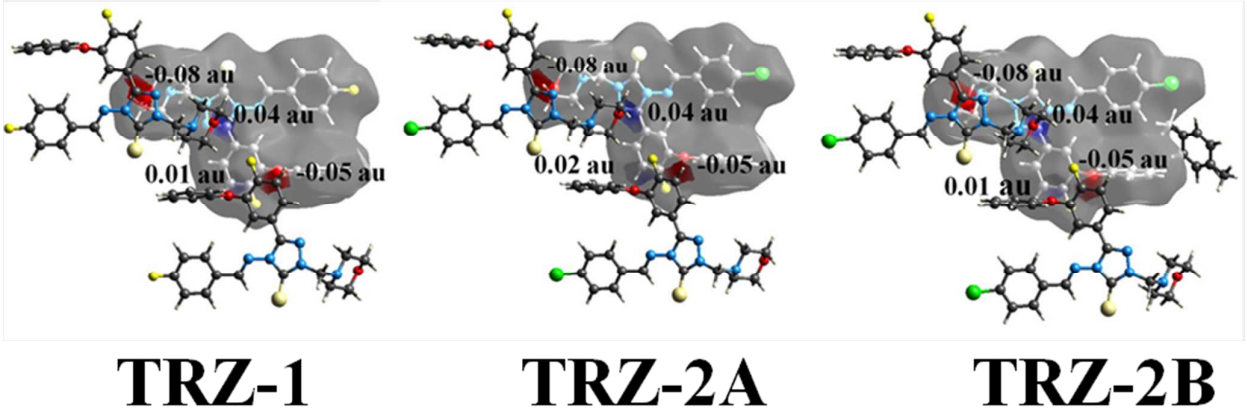

Figure-7: Decomposed ESP map plotted on Hirshfeld surface showing the contribution of both the O(*lp*)…π interactions along with the ESP values.

In case of S(*lp*)…π interaction, the electronegative region (ESP being -0.05 a.u.) around the sulphur atom was observed to interact with the electropositive region of Cg3 ring (ESP being 0.00 a.u.) in **TRZ-1 [Figure-8]**. Similar values of ESP were observed for **TRZ-2A**. This *lp*…π interaction was not observed in case of **TRZ-2B** and was replaced by a π- π stacking interaction **[Figure-8].**

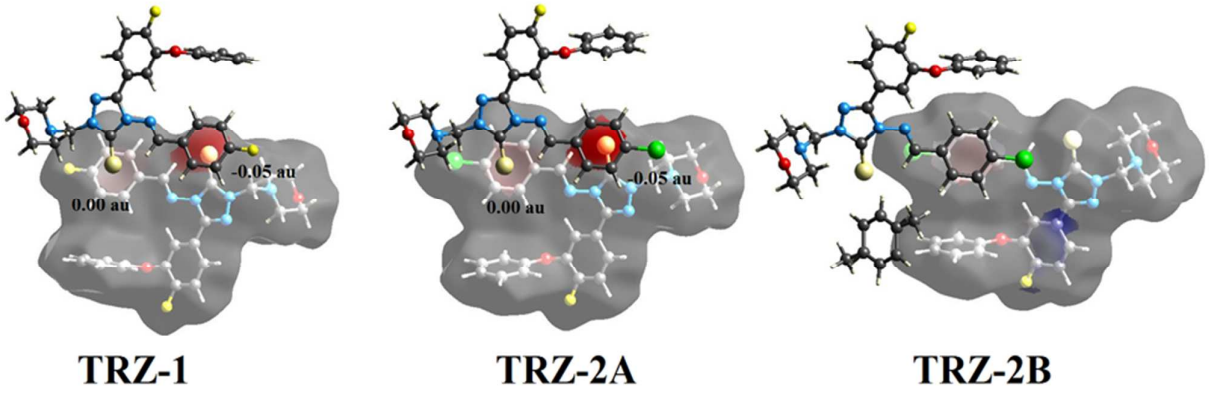

Figure-8: Decomposed ESP map plotted on Hirshfeld surface showing the contribution of S(*lp*)…π interactions in **TRZ-1** and **TRZ-2A** along with the respective ESP values and the presence of a π-π interaction in **TRZ-2B.**

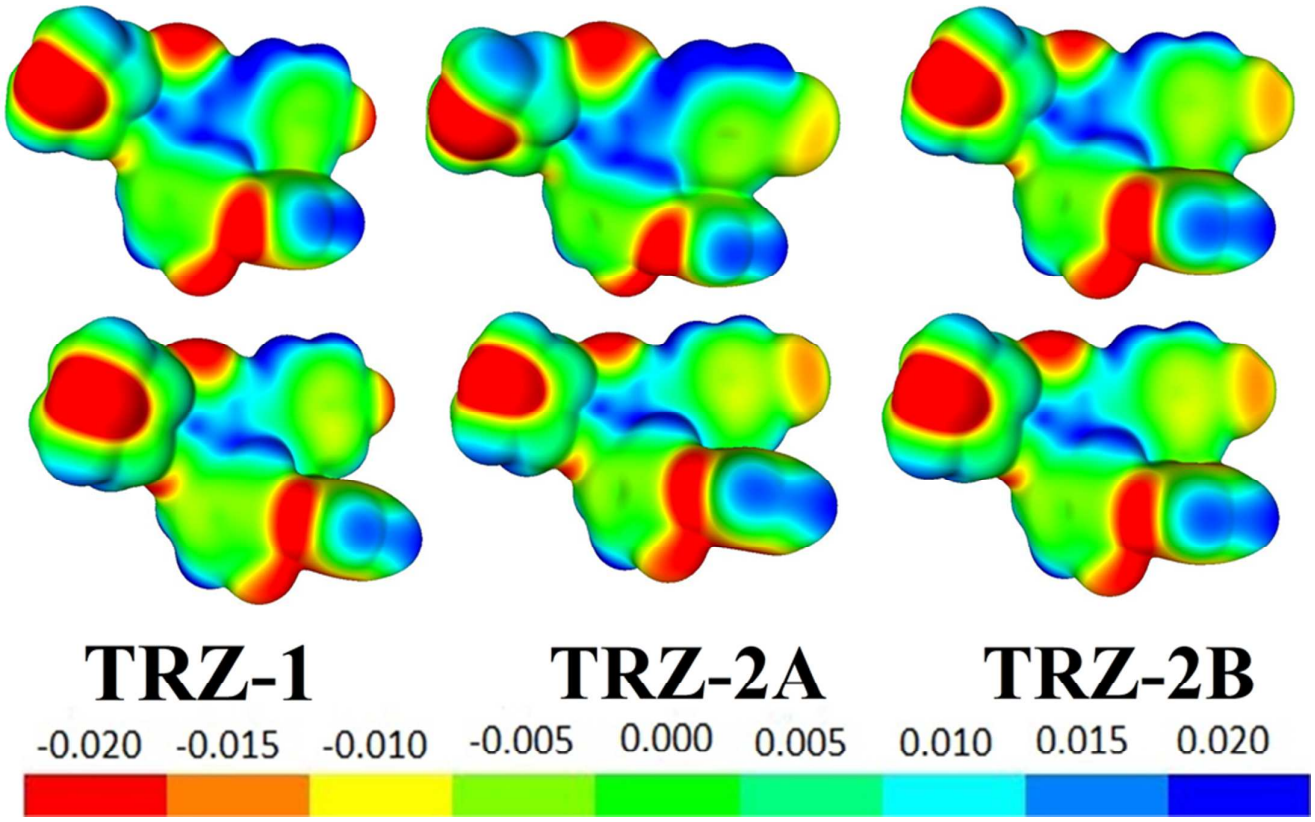

Figure-9: ESP plotted (in a.u.) on an isosurface of 0.0005 a.u. using gOpenMol at the solid state geometry (above) and optimized structure (below) with ESP ranging from red (electronegative region) to blue (electropositive region).

The ESP plotted using gOpenMol **[Figure-9]** on a isosurface of 0.0005 a.u. and with potential ranging from 0.02 a.u.(blue) to -0.02 a.u.(red) shows similar distribution of electronegative and electropositive region, similar to those observed in **Figures 6**. A comparison of the electropositive and electronegative regions of the ESP indicates that these are different in the solid state geometry when compared to the optimized geometry for **TRZ-1**, **TRZ-2A** and **TRZ-2B.**

The fingerprint plots for all the three structures have been shown in **[Figure-S12, ESI]**. Besides a few significant differences, the contributions of all the interaction were similar in all the three structures. It is of interest to note that the contribution of H…F interactions (15.1% for **TRZ-I**) was much higher than the H…O interaction (4.0% for **TRZ-1**) [**Figure-S12, ESI**]. Similar trends were observed in **TRZ-2A** and **TRZ-2B**. Also the contribution of H…F interaction was less in both **TRZ-2A** and **TRZ-2B** as compared to that of **TRZ-1**. This decrease in contribution of H…F interaction in both **TRZ-2A** and **TRZ-2B** was concomitantly replaced by H…Cl interaction **[Figure-S12, ESI].**

Previous studies on the O(*lp*)...π interaction have reported this kind of interaction but with reduced stability when compared to **TRZ-1** and **TRZ-2** [**48**]. Also, the S(*lp*)...π interaction with higher interaction energy compared to **TRZ-1** and **TRZ-2A** has been reported in literatures **[49]**. Since in our systems the *lp*… π interactions were found to be very stabilized and significant contributor towards crystal packing in all the crystal structures, it was of interest to analyse the decomposed finger print plots for these interactions in all the structures **[Figure-S12, ESI].** It was observed that the contribution of the O…C interactions were nearly comparable in all the three crystal structures, supporting the presence of *lp*…π interaction. The decomposition of the S…C interaction also clearly explained the presence of S(*lp*)…π in **TRZ-1** and **TRZ-2A** and its absence in **TRZ-2B**. The contribution of C…S interaction in **TRZ-2B** was observed to be 0% as compared 2.6% in case of both **TRZ-1** and **TRZ-2A (Figure-10)**. This absence in **TRZ-2B** is directly compensated by contribution from C…C interaction (π…π). In **TRZ-1** and **TRZ-2A**, this contribution is 2.7% and 2.8% respectively as compared to 4.8% in case of **TRZ-2B [Figure-10]**.

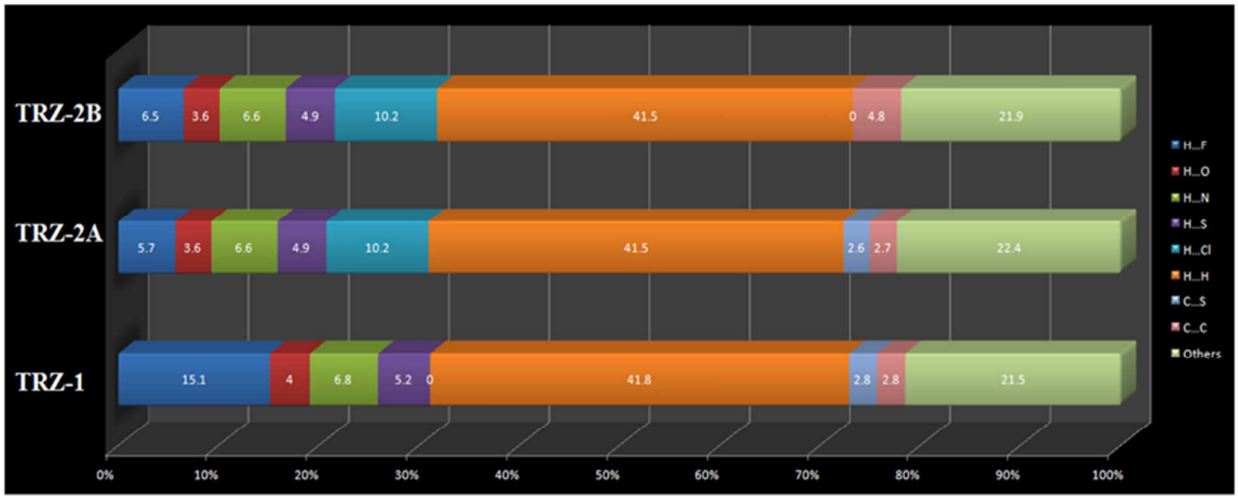

Figure-10: Percentage distribution of the different intermolecular interactions present in the three crystal structures.

Investigation of related crystal structures in CSD

Cambridge Structural Database (version 5.34) **[50]** search were also performed for derivatives of (*E*)-4-(benzylideneamino)-1-methyl-3-phenyl-1H-1,2,4-triazole-5(4H)-thione for only organic structures which are not ionic, polymeric, disordered and have their 3D coordinates determined. This resulted in 4 hits i.e **AZUTAR**[**51a**], **AZUTEV**[**51b**], **EXITUB**[**51c**], **ULIBAT[51d].** It is noteworthy that the molecular conformation is stabilized via C-H…S and C-H…N intramolecular interactions in all the 4

molecules [**Figure-11**]. The related relevant torsion angles for these molecules in the solid state and the optimized geometries reported in **Table-S4, ESI.**

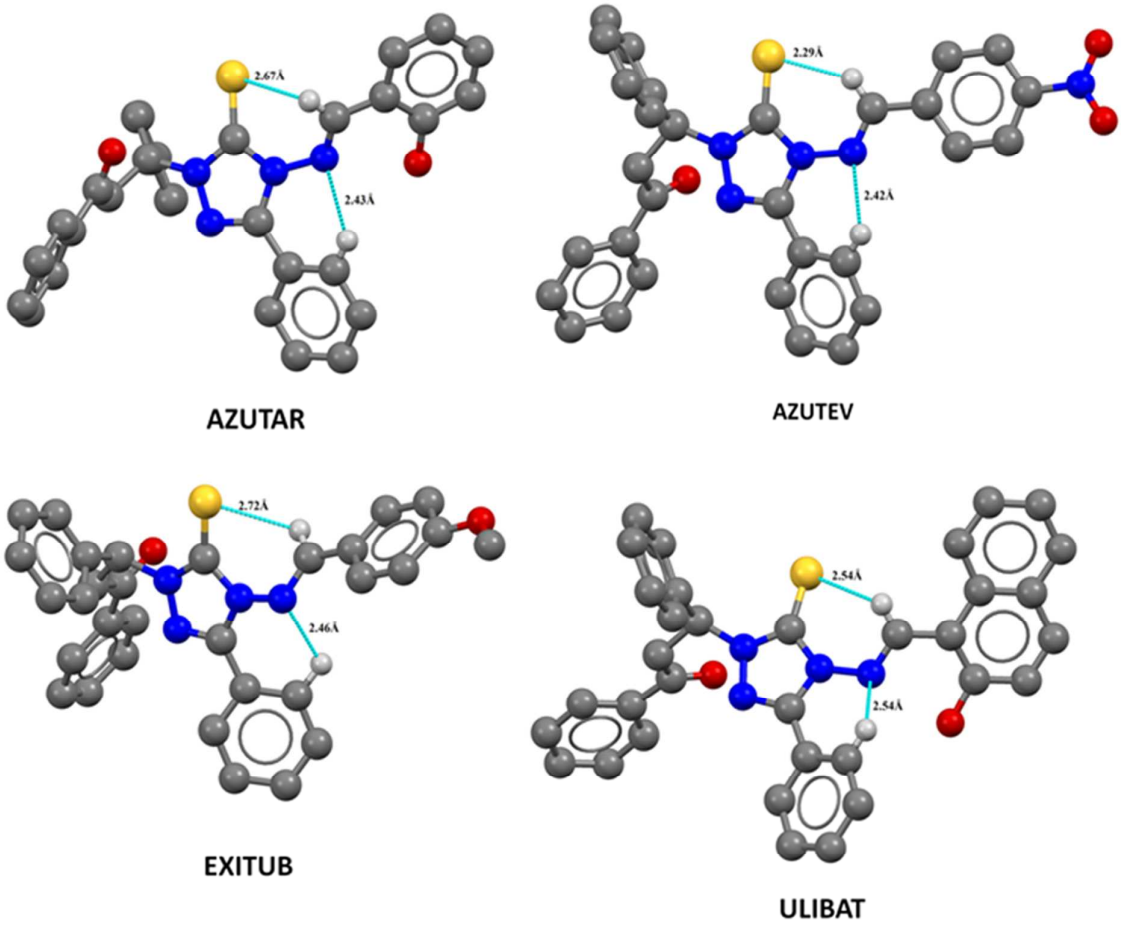

Figure-11: Structure of the molecule retrieved from CSD search with C-H…N and C-H…S intramolecular distance. Hydrogen atoms have been removed for clarity.

Conclusions

The synthesis and crystallographic analysis of two biologically active derivatives of 1,2,4-triazoles shows the presence of different intermolecular interactions participating in the crystal packing. It is of significance to realize that *lp*…π interactions play an important role in crystal packing their energies ranging from -4 kcal/mol to -12 kcal/mol depending on the availability of the *lp* of electrons on oxygen/sulfur atom and the calculated energies are commensurate with the magnitude of the ESP involving the *lp*…π regions. The order of availability of the lone pair electron density is maximum for the oxygen *lp* of the morpholine ring, followed by sulfur and then the oxygen atom of the fluorophenoxy ring. This indicates that the nature of the functional groups plays a pivotal role in

determining the energetics of a given interaction. The presence of weak C-H…F interactions also plays an important role in crystal packing in addition to the presence of C-H…Cl/O/S/π and stacking interactions. It is of interest to note the presence of the σ-hole in both the **TRZ-2A** and **TRZ-2B**, the differences indicating the varying extents of polarization of the molecule in the crystal field. The presence of such key supramolecular features in small molecules highlights the contributing role of weak intermolecular interactions in crystal packing. These are expected to have implications when such molecules bind with the active site of the enzyme resulting in modification in the biological function. It is also of interest to screen a molecule extensively for polymorphism and delineate the role of such weak interactions in crystal packing.

Acknowledgements: RS thanks DST-Fast Track for scholarship and Piyush Panini for his help on the theoretical calculations. DC thanks IISER Bhopal for infrastructure and research facilities and DST for financial support.

References

1. G. R. Desiraju, *J. Am. Chem. Soc*, 2013, **135**, 9952.
2. G. R. Desiraju, *Angew. Chem. Int. Ed.*, 2007, **46**, 8342.
3. (a) S. P. Thomas, M. S. Pavan and T. N. Guru Row, *Cryst. Growth Des.*, 2012, **12**, 6083; (b) M. Mazik, D. Bläser and R. Boese, *Tetrahedron*, 2001, **57**, 5791; (c) G.R. Desiraju*, Chem. Commun.*, 2005, 2995; (d) E. Bosch, *Cryst. Growth Des.*, 2010, **10**, 3808.
4. (a) P. Panini and D. Chopra, *CrystEngComm*, 2012, **14**, 1972; (b) P. Panini and D. Chopra, *CrystEngComm*, 2013, **15**, 3711; (c) G. Kaur, P. Panini, D. Chopra and A. R. Choudhury, *Cryst. Growth Des*., 2012, **12**, 5096; (d) V. R. Hathwar, S. M. Roopan, R. Subhasini, F. N. Khan and T. N. Guru Row, *J. Chem. Sci.,* 2010, **122**, 677; (e) M. Karanam and A. R. Choudhury, *Cryst. Growth Des*., 2013, doi.10.1021/cg400967k; (f) D. Trybiński and A. Sikorski, *CrystEngComm,* 2013, **15**, 6808.
5. (a) M. Nishio, Y. Umezawa, K. Honda, S. Tsuboyama and H. Suezawa*, CrystEngComm*, 2009, **11**, 1757; (b) O. Takahashi, Y. Kohno and M. Nishio, *Chem. Rev*., 2010, **110**, 6049; (c) M. Nishio, *Phys. Chem. Chem. Phys.*, 2011, **13**, 13873.
6. (a) C. R. Martinez and B. L. Iverson, *Chem. Sci.*, 2012, **3**, 2191; (b) J. F. Gonthier, S. N. Steinmann, L. Roch, A. Ruggi, N. Luisier, K. Severin and C. Corminboeuf, *ChemCommun.*, 2012, **48**, 9239.
7. (a) A. Robertazzi, F. Krull, E. W. Knapp and P. Gamez, *CrystEngComm*, 2011, **13**, 3293; (b) A. Jain, V. Ramanathan and R. Sankararamakrishnan, *Protein Sci.,* 2009, **18**, 595.
8. (a) K. Hiraoka, S. Mizuse and S. Yamabe, *J. Phys. Chem*., 1987, **91**, 5294; (b) M. Egli and R. V. Gessner, *Proc. Natl. Acad. Sci.*, 1995, **92**, 180.
9. M. Egli and R. Sarkhel, *Acc. Chem. Res.*, 2007, **40**, 197.
10. D. X. Wang and M.X. Wang, *J. Am. Chem. Soc.*, 2013, **135**, 892.

11. M.A. AlDamen and M.S. Mubarak, *Struct. Chem.,* 2013, **24**, 215.
12. T. J. Mooibroek, P. Gamez and J. Reedijk, *CrystEngComm,* 2008, **10**, 1501.
13. M. J. Bialek, J. K. Zareba, J. Janczak and J. Zoń, *Cryst. Growth Des.*, 2013, **13**, 4039.
14. G. L. Perlovich, S. V. Blokhina, N. G. Manin, V. Volkova and V. V. Tkachev*, J. Therm. Anal Calorim.,* 2013, **111**, 655.
15. G. R. Desiraju, J. J. Vittal, A. Ramanan, *Crystal Engineering: A Textbook, World Scientific Publishing Co. Pvt. Ltd.*, 1st Ed., 2011.
16. (a) S. Busi, R. Fröhlich, M. Lahtinen, R. Sillanpää and K. Rissanen, *Z. Naturforsch*, 2007, **62b**, 35; (b) G. Dutkiewicz, B. Narayana, K. Veena, H. S. Yathirajan and M. Kubicki, *Acta Cryst. E*, 380-388, **67**, o334.
17. T. P. Mohan, *PhD Thesis*, Mangalore University, 2006.
18. H. Betkaş, Ş. Ceylan, N. Demirbaş, Ş. A. Karaoğlu and B. Sökmen, *Med. Chem. Res.*, 2013, **22**, 3629.
19. (a) J. D. Dunitz and A. Gavezzotti*, Cryst. Growth Des.*, 2012, **12**, 5873; (b) L. Maschio, Civalleri, P. Ugliengo and A. Gavezzotti, *J. Phys. Chem. A*, 2011, **115**, 11179; (c) J. D. Dunitz and A. Gavezzotti, *Chem. Soc. Rev.*, 2009, **38**, 2622; (d) J. D. Dunitz and A. Gavezzotti, *Cryst. Growth Des*., 2005, **5**, 2180; (e) J. D. Dunitz and A. Gavezzotti, *Angew. Chem, Int. Ed.*, 2005, **44**, 1766; (f) L. Carlucci and A. Gavezzotti, *Chem. Eur. J.,* 2005, **11**, 271; (g) A. Gavezzotti, *CrystEngComm*, 2003, **5**, 429; (h) A. Gavezzotti, *CrystEngComm*, 2003, **5**, 439.
20. (a) R. Ahlrichs, M. Baer, M. Haeser, H. Horn and C. Koelmel, Electronic structure calculations on work- station computers: the program system TURBOMOLE, *Chem. Phys. Lett.,* 1989, **162**, 165–169; (b) TURBOMOLE V6.3 2011, a development of University of Karlsruhe and Forschungszentrum Karlsruhe GmbH, 1989–2007, TURBOMOLE GmbH, since 2007, available from http:// www.turbomole.com.
21. (a) M. A. Spackman and D. Jayatilaka, *CrystEngComm*, 2009, **11**, 19; (b) J. J. McKinnon, D. Jayatilaka and M. A. Spackman*, Chem. Commun.*, 2007, 3814; (c) S. K. Wolff, D. J. Grimwood, J. J. McKinnon, M. J. Turner, D. Jayatilaka and M. A. Spackman, CrystalExplorer (Version 3.0), University of Western Australia, 2012.
22. D. Dey, T. P. Mohan, B. Vishalakshi, D. Chopra (Manuscript under preparation), 2013.
23. V. Petricek, M. Dusek and L. Palatinus, Jana2000, 08/11/2007, Institute of physics, Praha, Czech Republic, 2007.
24. A. Altomare, G. Cascarano, C. Giacovazzo and A. Guagliardi, *J. Appl. Crystallogr.*, 1993, **26**, 343.
25. G. M. Sheldrick, *Acta Crystallogr.,* 2007, **A64**, 112.
26. L. J. Farrugia, *J. Appl. Crystallogr.*, 1999, **32**, 837.
27. L. J. Farrugia, *J. Appl. Crystallogr.*, 1997, **30**, 565.
28. C. F. Macrae, I. J. Bruno, J. A. Chisholm, P. R. Edgington, P. McCabe, E. Pidcock, L. Rodriguez-Monge, R. Taylor, J. Streek and P. A. Wood, *J. Appl. Crystallogr.*, 2008, **41**,466, www.ccdc.cam.ac.uk/mercury.
29. M. Nardelli*, J. Appl. Crystallogr.*, 1995, **28**, 659.
30. A. L. Spek, *Acta Crystallogr.,* 2009, **D65**, 148.
31. (a) A. Gavezzotti, *New J. Chem.*, 2011, **35**, 1360; (b) A. Gavezzotti, *J. Phys. Chem. B*, 2003, **107**, 2344; (c) A. Gavezzotti, *J. Phys. Chem. B*, 2002, **106**, 4145.

32. (a) S. Grimme, J. Antony, S. Ehrlich and H. Krieg, *J. Chem. Phys.,* 2010, **132**, 154104; (b) J. Moellmann and S. Grimme, *Phys. Chem. Chem. Phys*., 2010, **12**, 8500; (c) W. Hujo and S. Grimme, *Phys. Chem. Chem. Phys.*, 2011, **13**, 13942.
33. S. Grimme, *J. Comput. Chem.*, 2006, **27**, 1787.
34. L. Laaksonen, A graphics program for the analysis and display of molecular dynamics trajectories. *J. Mol. Graph.* 1992, **10,** 33-34. (b) D.L. Bergman, Laaksonen, L. Laaksonen and A. Laaksonen, Visualization of solvation structures in liquid mixtures. *J. Mol. Graph. Model.* 1997, **15,** 301-306.
35. Gaussian 03, Revision C.02, M. J. Frisch, G. W. Trucks, H. B. Schlegel, G. E. Scuseria, M. A. Robb, J. R. Cheeseman, J. A. Montgomery, Jr., T. Vreven, K. N. Kudin, J. C. Burant, J. M. Millam, S. S. Iyengar, J. Tomasi, V. Barone, B. Mennucci, M. Cossi, G. Scalmani, N. Rega, G. A. Petersson, H. Nakatsuji, M. Hada, M. Ehara, K. Toyota, R. Fukuda, J. Hasegawa, M. Ishida, T. Nakajima, Y. Honda, O. Kitao, H. Nakai, M. Klene, X. Li, J. E. Knox, H. P. Hratchian, J. B. Cross, V. Bakken, C. Adamo, J. Jaramillo, R. Gomperts, R. E. Stratmann, O. Yazyev, A. J. Austin, R. Cammi, C. Pomelli, J. W. Ochterski, P. Y. Ayala, K. Morokuma, G. A. Voth, P. Salvador, J. J. Dannenberg, V. G. Zakrzewski, S. Dapprich, A. D. Daniels, M. C. Strain, O. Farkas, D. K. Malick, A. D. Rabuck, K. Raghavachari, J. B. Foresman, J. V. Ortiz, Q. Cui, A. G. Baboul, S. Clifford, J. Cioslowski, B. B. Stefanov, G. Liu, A. Liashenko, P. Piskorz, I. Komaromi, R. L. Martin, D. J. Fox, T. Keith, M. A. Al-Laham, C. Y. Peng, A. Nanayakkara, M. Challacombe, P. M. W. Gill, B. Johnson, W. Chen, M. W. Wong, C. Gonzalez, and J. A. Pople, Gaussian, Inc., Wallingford CT, 2004.
36. M. Abe, M. Eto, K. Yamaguchi, M. Yamasaki, J. Misaka, Y. Yoshitake, M. Otsuka and K. Harano, *Tetrahedron*, 2012, **68**, 3566.
37. K. A. Solanko and A. Bond, *Acta Cryst.*, 2011, **B67**, 437.
38. (a) D. Chopra and T. N. Guru Row, *Cryst. Growth Des.*, 2008, **8**, 848. (b) D. Chopra and T. N. Guru Row, *Cryst. Growth Des.*, 2005, **5**, 1679. (c) D. Chopra and T. N. Guru Row, *Cryst. Growth Des.*, 2006, **6**, 1267.
39. D. Chopra and T. N. Guru Row, *CrystEngComm*, 2008, **10**, 54.
40. (a) D. Chopra, V. Thiruvenkatam and T. N. Guru Row, *Cryst Growth & Des.*, 2006, **6**, 843. (b) J. Ridout and M. R. Probert, *Cryst Growth & Des.*, 2013, **13**, 1943. (c) A. R. Choudhury, N. Winterton, A. Steiner, A. I. Cooper and K. A. Johnson, *J. Am. Chem. Soc.*, 2005, **127**, 16792.
41. (a) C-H…N interaction: H. Roohi and S. Bagheri, *Int. J. Quant. Chem.*, 2011, **111**, 961. (b) C-H…S interaction: E. M. C. Lago, J. M. H. Ramòn and J. R. Otero*, J. Phys. Chem. A*, 2004, **108**, 4923. (c) C-H…O interaction: Estimating the exact contribution of C-H…O interaction in the molecular pair is very difficult because it is present along with other intermolecular interactions such as C-H…F and stacking interaction resulting in a very high stability of the molecular pairs in which C-H…O is present. In one reference it has been reported that the energy of C-H…O interaction may be around -5 kcal/mol. B. Wang, J. F. Hinton and P. Pulay, J. Phys. Chem. A, 2003, 107, 4683.

42. (a) A. Kálmán, L. Párkányi, G. Argay, *Acta Crystallogr*., 1993, **B49**, 1039. (b) T. Gruber, P. Bombicz, W. Seichter and E. Weber, *J. Struct. Chem.*, 2009, **50**, 522.
43. T. Gelbrich, T. L. Threlfall and M. B. Hursthouse, *CrystEngComm*, 2012, **14**, 5454.
44. (a) T. Gelbrich and M. B. Hursthouse, *CrystEngComm*, 2005, **7**, 324; (b) T. Gelbrich and M. B. Hursthouse, *CrystEngComm,* 2006, **8**, 448.
45. (a) D. Chopra, V. V. Zhurov, E. A. Zhurova and A. A. Pinkerton, *J. Org. Chem.*, 2009, **74**, 2389-2395. (b) M. A. Spackman, J. J. McKinnon and D. Jayatilaka, *CrystEngComm*, 2008, **10**, 377.
46. A. Bauzá, D. Quinonero, P.M. Deyá and A. Frontera, *CrystEngComm*, 2013, **15**, 3137.
47. (a) G. R. Desiraju and R. Parthasarathy, *J. Am. Chem. Soc*., 1989, **111**, 8725; (b) V. R. Hathwar and T. N. Guru Row, *J. Phys. Chem. A*, 2010, **114**, 13434.
48. (a) J. C. Amicangelo, D. G. Irwin, C. J. Lee, N. C. Romano and N. L. Saxton, *J. Phys. Chem. A*, 2013, **117**, 1336; (b) B. W. Gung, Y. Zou, Z. Xu, J. C. Amicangelo, D. G. Irwin, S. Ma and H. Zhou, *J. Org. Chem*., 2008, **73**, 689.
49. S. Yan, S. J. Lee, S. Kang, K. Choi, S. K. Rhee and J. Y. Lee, *Bull. Korean Chem. Soc*., 2007, **28**, 959.
50. (a) F. H. Allen*, Acta Cryst.*, 2008, **B58**, 380; (b) J. van de Streek, *Acta Cryst.*, 2006, **B62**, 567; (c) A. G. Orpen, *Acta Cryst.*, 2002, **B58**, 398; (d) F. H. Allen and W. D. S. Motherwell, *Acta Cryst.*, 2002, **B58**, 407. (e) R. Taylor, *Acta Cryst.*, 2002, **D58**, 879.
51. (a) Q. Liu, W. Wang, Y. Gao, J. Zhang, X. Jia, *Acta Crystallogr.*, 2011, **E67**, o2726; (b) W. Wang, Y. Gao, C. Xu, W. Wu, Q. Liu, *Acta Crystallogr.,* 2011, **E67**, o2727; (c) W. Wang, Q. Liu, Y. Gao, X. Jia, J. Jhang, *Acta Crystallogr.,* 2011, **E67**, o2534; (d) W. Wang, H. Yao, Y. Gao, J. Zhang, X. Jia, *Acta Crystallogr.,* 2011, **E67**, o675.

Graphical Abstract

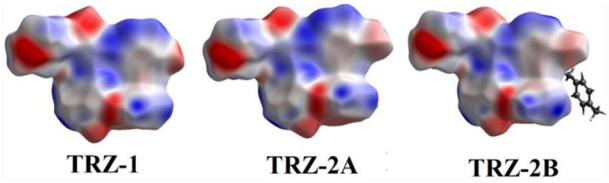

The calculations performed on the evaluation of the electrostatic potential render deeper insights into the nature of *lp*…π interactions